

Simulation of Climate Changes in the 20th–22nd Centuries with a Coupled Atmosphere–Ocean General Circulation Model

E. M. Volodin and N. A. Diansky

Institute of Numerical Mathematics, Russian Academy of Sciences, ul. Gubkina 8, Moscow, 119991 Russia
e-mail: volodin@inm.ras.ru

Received March 30, 2005; in final form, September 20, 2005

Abstract—The results of numerical experiments with a coupled atmosphere–ocean general circulation model on the reproduction of climate changes during the 20th century and on the simulation of possible climate changes during the 21st–22nd centuries according to three IPCC scenarios of variations in the concentrations of greenhouse and other gases, as well as the results of the experiments with the doubled and quadruple concentrations of CO₂, are considered. An increase in the near-surface air temperature during the 20th century and the features of the observed climate changes, such as warming in 1940–1950 and its slowing down in 1960–1970, are adequately reproduced in the model. According to the model, the air-temperature increase during the 22nd century (as compared to the end of the 20th century) varies from 2 K for the most moderate scenario to 5 K for the warmest scenario. This estimate is somewhat lower than the expected warming averaged over the data of all models presented in the third IPCC report. According to model data, in the 22nd century, under all scenarios, at the end of summer, a complete or almost complete sea-ice melting will occur in the Arctic. According to the model, by the year 2200, the sea level will vary by 20 to 45 cm as compared to the level at the end of the 20th century.

DOI: 10.1134/S0001433806030017

INTRODUCTION

One of the most important problems of modern climatology is the problem of predicting climate changes during the next few centuries. In the narrow sense, we will define climate in accordance with the definition adopted in the IPCC report [1], where climate is defined as a statistical description with respect to the mean values and variability of the corresponding quantitative indicators (climate characteristics) over a time period of a few months to thousands or millions of years. (The IPCC is the Intergovernmental Panel on Climate Change established in 1988 under the aegis of the World Meteorological Organization (WMO).) According to the WMO definition, the classical averaging period is 30 years (1961–1990 with reference to the current state). In most cases, these quantitative indicators are surface characteristics, such as air temperature, precipitation, wind, etc. In a wider sense, climate is an ensemble of states that the climate system has passed through over a sufficiently long period of time [2].

According to the IPCC report [1], the observed significant climate changes are primarily due to anthropogenic forcing mainly related to the atmospheric emissions of greenhouse gases, aerosols, and other pollutants. The only instrument providing quantitative estimates of future climate changes is a numerical model of the Earth's climate system. The understanding of the system's energy balance at a base level

implies that the simple models of the Budyko type [3] can provide a rough quantitative estimate of some globally averaged climate characteristics. However, more accurate estimates of feedbacks and regional details can be obtained only with the aid of combined climate models [1].

The complex character of the processes occurring in the climate system does not allow the use of extrapolations of historical trends or statistical and other purely empirical methods to obtain long-term estimates. Therefore, at present, the Coupled Model Intercomparison Project (CMIP; see <http://www-pcmdi.llnl.gov/projects/cmip/index.php>) is being performed to compare the climate-change predictions obtained with different climate models under the scenarios proposed in [1] for possible future variations in the atmospheric concentrations of greenhouse gases, aerosols, and other pollutants. This program is a step forward as compared to a similar comparison [4] that was carried out in 2001 and whose results were reflected in the third IPCC report [1]. The results obtained in the course of this program will be reflected in the fourth IPCC report. Now, a greater number of models take part in the comparison; each of them has been improved.

The objective of this study is to analyze the responses of the coupled atmosphere–ocean general circulation model developed at the Institute of Numerical Mathematics, Russian Academy of Sciences

(INM RAS), to possible future variations in anthropogenic forcing. These responses were obtained from a series of experiments carried out in the CMIP framework under the scenarios taken from [1]. These experiments were carried out with a new version of the coupled model as compared to that described in [5]. A detailed description of the differences between the new version of the coupled model and that described in [5] is given in [6, 7].

In [8], the response of the previous version of the INM coupled atmosphere–ocean model [5] to an increase in CO₂ concentration in the atmosphere was analyzed and compared with the results obtained with other models. Here, the response to a prescribed increase in CO₂ concentration was studied by comparing two 80-year calculations made according to the scenario proposed in the CMIP2 project (see <http://www-pcmdi.llnl.gov/projects/cmip/index.php>). In the first (control) experiment, the atmospheric CO₂ concentration was set constant and equal to its value observed in the late 20th century. In the second experiment, the concentration of CO₂ was increased by 1% per year.

The experiments presented in this study were carried out according to more complicated and realistic scenarios with a new improved version of the INM RAS coupled general circulation model, whose sensitivity to external forcing was increased by more than 1.5 times (see below). In Russia, such experiments with the coupled atmosphere–ocean general circulation model were carried out for the first time. In the following sections, a short description of the new version of the INM coupled model is given, the methods of conducting such experiments are described, and the results obtained are analyzed and compared with the data given in the third IPCC report [1]. In one of the experiments, in addition to the coupled atmosphere–ocean general circulation model, an atmospheric model coupled with a simple balance model of the heat content of a homogeneous 50-m ocean layer is used. Although the correction of heat fluxes at the ocean surface is used, this model makes it possible to promptly obtain an equilibrium response to a prescribed external forcing and also to emphasize the role of ocean circulation.

1. DESCRIPTION OF THE COUPLED MODEL AND NUMERICAL EXPERIMENTS

A new version of the coupled atmosphere–ocean general circulation model developed at the INM RAS was used to simulate climate changes. The previous model is described in detail in [5], and its modifications are described in [6, 7]. Here, we will give its short description.

A complete description of the atmospheric general circulation model is given in [9]. The spatial resolu-

tion for the atmospheric block is 5° in longitude, 4° in latitude, and 21 levels in the vertical in the σ -coordinates. The equations of hydrothermodynamics are solved on a “C” grid according to the Arakawa classification with the use of the finite-difference method described in [10]. The model involves the parameterizations of radiation processes [11], convection, and condensation [12]; the processes occurring in soil and on the dry-land surface [13]; and gravity-wave resistance [14, 15].

A detailed description of the ocean general circulation model and its features is given in [16, 17]. The model is based on the ocean primitive equations in the Boussinesq, hydrostatic, and rigid-lid approximations written in a spherical isobathic σ -coordinate system. Its resolution is 2.5° × 2° in longitude and latitude, respectively, and 33 nonuniform levels in depth. The discretization of dynamics equations was performed on a C grid with low dissipation. The use of the C grid at the resolution 2.5° × 2° allows one to approximate the calculation region for straits. For example, it is possible to describe the salt exchange between the Atlantic and the Mediterranean Sea through the Strait of Gibraltar, a procedure that is very important for the description of a thermohaline circulation in the North Atlantic, and the exchanges through the Bering Strait as well. In implementing the model numerically, the method of splitting up [18] in physical processes and spatial coordinates is used. This method allows one to efficiently realize implicit methods of time integration. The vertical viscosity and diffusion are parameterized according to [19]. The model also involves a block of sea-ice calculation [20], in which the thermodynamics of ice is taken into account but its motion is disregarded.

Data exchange between the atmosphere and ocean models occurs every 6 h of model time. This interval is also used as a numerical step of the ocean model. Within this interval, the calculated (with the atmosphere model with a step of 1 h) fluxes of sensible and latent heat, freshwater, momentum, and total (incoming and outgoing) long- and shortwave radiation at the ocean surface are accumulated and then averaged. The fields are converted from the atmospheric spatial grid to the oceanic grid with the aid of linear interpolation. Since the spatial oceanic grid is denser than the atmospheric grid, the spatial weight averaging procedure was used to convert the ocean surface temperature (OST) to the atmospheric grid. The latter implies that the OST at all oceanic grid points falling within a mesh of the atmospheric grid is taken with a weight proportional to the area of intersection of the corresponding oceanic mesh with the mesh of the atmospheric grid. No correction of the heat and momentum fluxes is used in adjusting the atmosphere and ocean models. The correction of the freshwater flux is used only for the Greenland, Norwegian, Barents, and Kara

seas. Such a correction makes it possible to reproduce a thermohaline circulation in the northern Atlantic more adequately and does not directly affect the hydrologic-cycle elements, such as precipitation, river runoff, etc. In calculating fluxes at the ocean surface in the atmosphere model, the OST is taken from the uppermost calculation level in the ocean model.

The coupled atmosphere–ocean general circulation model is implemented in a 16-processor cluster (Intel Itanium) at the INM RAS. Calculations with eight processors for 10 model years take 24 h.

The reproduction of the climate of the late 20th century with this coupled model is described in [7].

In the experiments, in addition to the coupled atmosphere–ocean general circulation model, an atmosphere model coupled with a simple balance model of the heat content of a homogeneous 50-m ocean layer is used. Additionally, this model also involves the calculation of sea ice and uses the correction of heat fluxes at the ocean surface. Such a simplified coupled model allows prompt obtainment of an equilibrium response to a prescribed external forcing, for example, to an increase in the CO₂ concentration.

The following experiments with the coupled model were carried out in the CMIP framework.

1. Experiment on simulation of the climate of the 20th century (experiment 20). The initial state for this experiment was obtained in the following way. First, in the ocean model, temperature and salinity were specified according to the observational data given in [21], flow velocities were zero, the amount of sea ice was equal to zero, and the atmospheric condition was taken from the integration of the atmosphere model with a specified OST distribution. From this initial state, the model was integrated for 160 years; in this case, the concentrations of all atmospheric components corresponded to those of the end of the 20th century. Then, the calculations were performed for 80 years, and, in this case, the concentrations of all atmospheric constituents corresponded to those of the year 1871. The state of the model at the end of the calculations was starting for experiment 20. In the course of this experiment, real time variations in the atmospheric concentrations of carbon dioxide (CO₂), methane (CH₄), and nitrogen monoxide (N₂O)—major greenhouse gases associated with man's activities—were specified. These gases were assumed to be well mixed, and their concentrations did not depend on the spatial coordinates. Real time variations in the sulfate-aerosol concentration depending on latitude and longitude, the volcanic-aerosol optical depth depending on latitude, and the solar constant were also specified. In the model, only the direct effect of sulfate aerosol was taken into account. In the INM model, the direct radiation effect of variations in the concentration of sulfate aerosol during the 20th century was approxi-

mately 1.5 times larger than its mean value given in [1] and was equal to -0.75 W/m^2 . Figure 1 gives the temporal behaviors of all external forcings used. The data were taken from the Internet at http://www-pcmdi.llnl.gov/ipcc.climate_forcing.php. The duration of experiment 20 was 130 years; i.e., the calculation was performed to the end of the year 2000.

2. Experiments on simulation of the climate of the 21st–22nd centuries. In these experiments, the initial data were taken from the model state obtained at the end of experiment 20, which corresponded to the beginning of the year 2001. The atmospheric concentrations of carbon dioxide, methane, nitrogen monoxide, and sulfate aerosol in the 21st century corresponded to those from IPCC scenarios A1B, A2, and B1 (Fig. 1). Therefore, these experiments will be denoted according to the scenario abbreviations. The solar constant and the concentrations of volcanic aerosols were set constant and equal to their values observed in 2000. During the 22nd century, the concentrations of all gas constituents corresponded to their values for the year 2100. The duration of each of these experiments was 200 years.

3. Experiment 21 on the simulation of the climate of the 21st century under the assumption that the concentrations of all gases corresponded to their values observed in 2000. The model state for the end of experiment 20 was used as the initial state. The duration of the experiment was 100 years.

4. Control experiment 80, in which the concentrations of all gases and the solar constant corresponded to their values for the year 1871. The same initial state was used as that for experiment 20. The duration of the experiment was 330 years.

5. Experiment 2CO₂, in which the CO₂ concentration was increased at a rate of 1% per year up to its doubling (during 70 years), plus 150 calculation years with doubled CO₂. The concentrations of the rest of the gases were set constant. The same initial state was used as for experiment 20. The duration was 220 years.

6. Experiment 4CO₂, in which the CO₂ concentration was increased at a rate of 1% per year up to its quadrupling (during 140 years), plus 150 years of calculation with quadruple CO₂. The same initial state was used as for experiment 20. The duration was 290 years.

7. Experiment SLC on simulation of the climate of the late 20th century via a model with a 50-m ocean. The duration of the experiment was 60 years, excluding 20 years during which an equilibrium climate was reached.

8. Experiment different from the SLC experiment by doubled CO₂. The duration of the experiment was 60 years, excluding 20 years during which an equilibrium climate was reached.

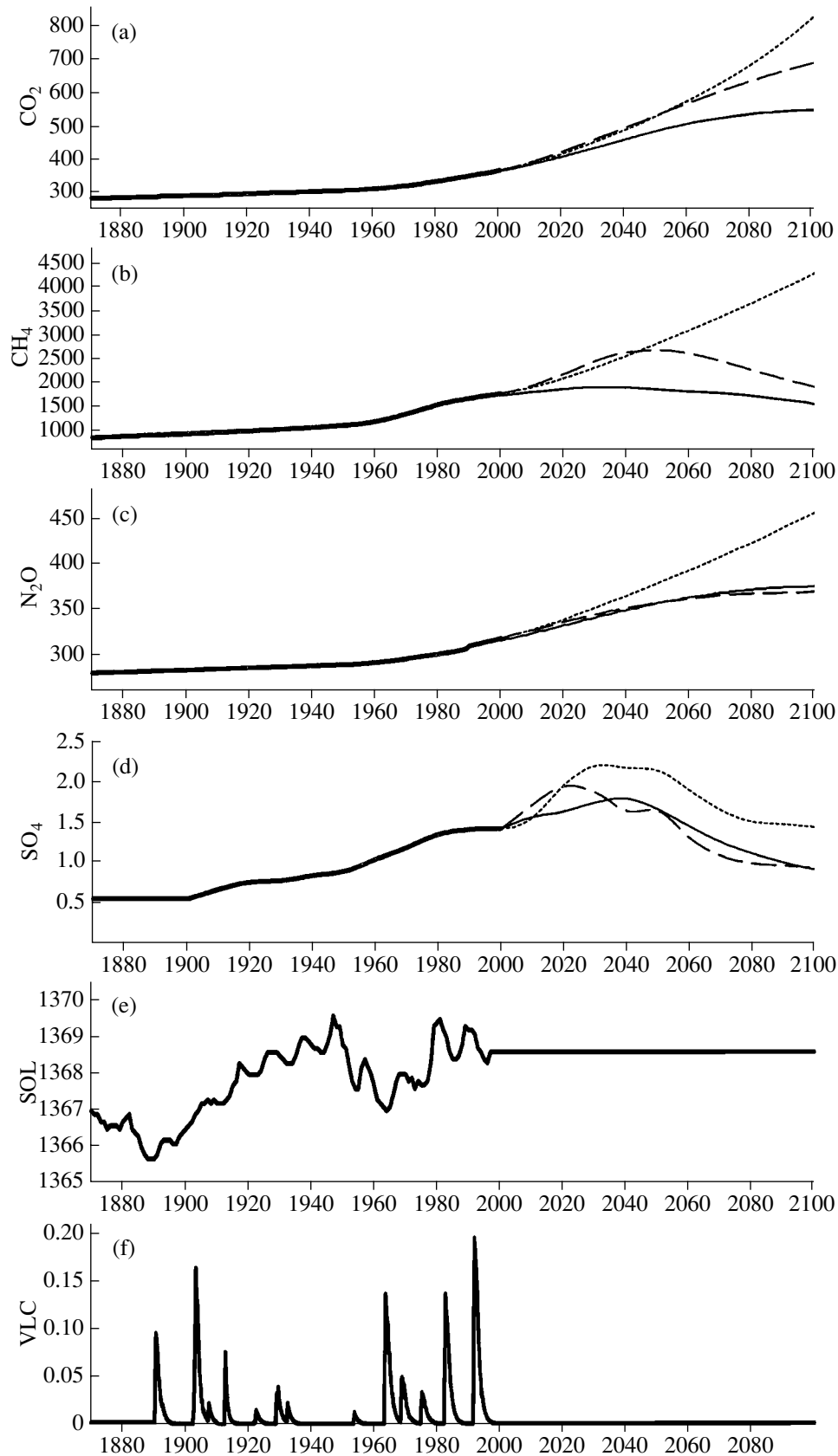


Fig. 1. Variations in the concentrations of (a) carbon dioxide (ppm), (b) methane (ppb), (c) nitrogen monoxide (ppb), (d) integral sulfate aerosol (mg/m^2), (e) solar constant (W/m^2), and (f) integral optical thickness of volcanic aerosol (dimensionless) in (thick solid curve) experiments 20, (thin solid curve) B1, (dashed curve) A1B, and (dotted curve) A2.

2. RESULTS OF NUMERICAL EXPERIMENTS

The sensitivity of a climate model to an increase in the concentrations of greenhouse gases is characterized primarily by an increase in globally averaged surface air temperature under CO_2 increased by 1% per year up to its doubling and by an equilibrium increase in surface air temperature under doubled CO_2 in the model with a homogeneous 50-m ocean layer. In the INM model, according to the data obtained from the experiment with CO_2 increased by 1% per year, warming is 1.57 K under doubled CO_2 (years 61–80) as compared to the same years of the control experiment. This value is close to the mean (1.61 K) over all models participating in similar experiments in the CMIP framework [4, 22]. The scatter in the data obtained with the models is sufficiently wide. For example, the minimum warming is 0.75 K, and the maximum warming is 3.77 K. However, the model experiments in the CMIP framework were carried out mainly in 2000–2001.

According to the latest data, for 12 models that participated in such an experiment in 2004, the average warming is 1.81 K, the minimum warming is 1.46 K, and the maximum warming is 2.2 K (Meehl, 2005, private communication). This implies that the average warming in the models is slightly increased and the scatter in model data is significantly decreased. In this experiment, the INM model yields a warming value that is slightly smaller than the mean over all models. For these 12 models, the value of equilibrium warming in the model with the upper ocean layer under doubled CO_2 is known. The average warming is 2.95 K, and, for different models, its value varies from 2.10 to 3.95 K. For the INM model, the equilibrium warming is 2.10 K, which is the smallest value among the models under consideration. Comparison between the equilibrium and nonequilibrium responses of the model suggests that, in the INM model with the entire ocean, a thinner ocean layer (as compared to other models) is responsible for warming. This reduces the disagreement between the INM model and the mean over all models in the nonequilibrium experiment. The reasons why the sensitivity to doubled CO_2 in the INM model is significantly lower than its mean over all models are analyzed in [22]. The main reason is an increase (under warming) in the amount of lower cloudiness under the conditions of a more frequent formation of inversion. In [22], the probable sensitivity of the real climate system is estimated.

As compared to the previous version of the INM coupled model [8], where the warming in the model with the entire ocean under CO_2 increased by 1% per year was 1.0 K, the model's sensitivity was increased by a factor greater than 1.5. This is primarily due to the introduction of an interactive model of sea ice. As compared to analogous years of the control experiment, the warming in the model with the entire ocean

under doubled CO_2 (experiment 2CO_2 , years 201–220) at the end of calculation is 2.1 K, which coincides with the value of equilibrium warming in the model with a 50-m ocean layer. By this moment, warming at the surface can be considered to be almost equilibrium. The fact that the values of the equilibrium warming in the models with the entire ocean and a 50-m ocean layer almost coincide suggests that it is possible to study the equilibrium sensitivity with the aid of the models with a 50-m ocean layer. At the end of the experiment with quadruple CO_2 (4CO_2 , years 271–290), the warming is 4.1 K as compared to analogous years of the control experiment. In this case, the warming at the surface can also be considered almost equilibrium. Comparison with the warming in the 2CO_2 experiment shows that the dependence of the equilibrium warming value on the logarithm of the CO_2 concentration increase is almost linear.

Let us consider the temporal behavior of the globally averaged air temperature at the surface in the control experiment, as well as in the experiments modeling the climate of the 20th–22nd centuries (Fig. 2). The mean air temperature for the control experiment is 12.6°C , which is 1.4°C below that obtained from the 1961–1990 observational data [23] and approximately 0.8 – 1.0°C below that obtained for the second half of the 19th century, for the conditions under which the control experiment was performed. In the control experiment, the temperature trend is positive; its value does not exceed 0.2 K over 330 years of the experiment. In the experiment simulating the climate of the 20th century, already by the mid-20th century, warming is noticeable as compared to the control experiment. The temperature rise reaches 0.7–0.8 K, which is close to the warming observed (0.6–0.7 K). In the data obtained from the control experiment, there is no time interval within which the warming would be equally significant. It follows that the warming of the 20th century is most likely caused not by the atmosphere–ocean system's variability, but by external (with respect to this system) forcings. The same conclusion is drawn from the results of other models [1].

According to our model, during the 21st century, even under all forcings fixed at a level of the year 2000 (experiment 21), warming is expected to be approximately 0.6 K owing to a large thermal inertia of the ocean. The rise of temperature in experiments B1, A1B, and A2 is more noticeable (as compared to the year 2000) and reaches 2, 3, and 5 K, respectively, by the end of the 22nd century according to model data. In experiment A2, a slight additional warming during the years 2145–2165 is due to variations in the time step in the atmospheric block of the model.

The temporal behavior of the globally averaged precipitation is shown in Fig. 2b for the experiments carried out. In the control experiment, the amount of

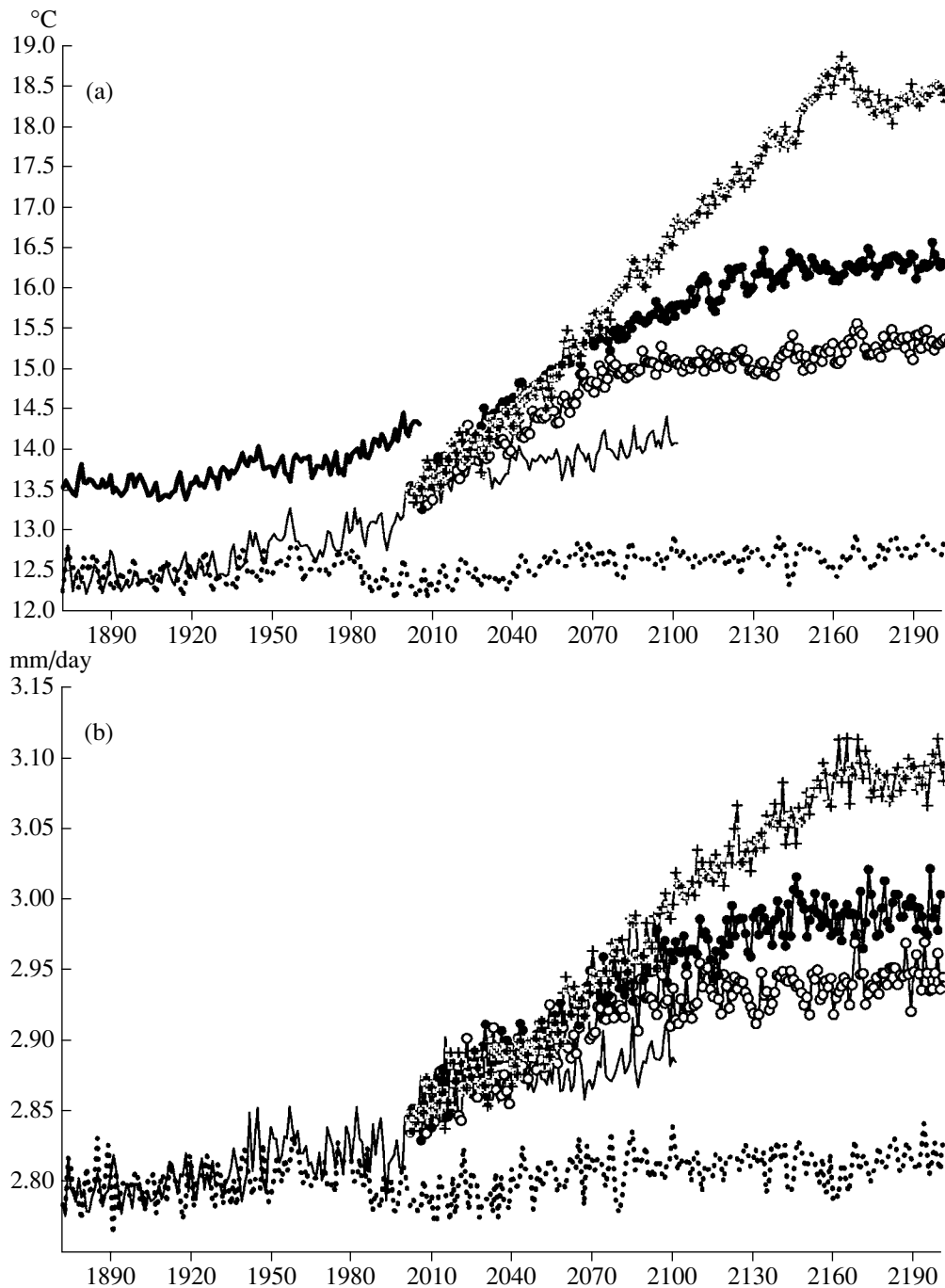


Fig. 2. Variations in (a) the integral temperature of surface air ($^{\circ}\text{C}$) and (b) precipitation (mm/day) for the (thick dotted curve) control experiment, (thin solid curve) experiments 20 and 21, (white circles) B1, (black circles) A1B, and (crosses) A2. The thick solid curve in Fig. 2a shows the observed temperature variation.

precipitation is about 2.80 mm/day. In experiment 20, the amount of precipitation is increased to 2.84 mm/day by the year 2000. By the end of experiment 21, the amount of precipitation is increased to 2.89 mm/day, and, by the end of experiments B1, A1B, and A2, the amount of precipitation is 2.95, 2.99, and 3.10 mm/day, respectively. In the experiments modeling warming, the amount of precipitation

is increased mainly in proportion to the increase of the mean air temperature at the surface.

Let us compare the temperature variation in experiment 20 with respect to the control experiment and the 1871–2000 temperature variation estimated from observational data [23] (Fig. 3). The model adequately reproduces the magnitude of warming in the 20th cen-

tury, which is about 0.6–0.7 K according to observational data. The features such as the warming in 1940–1950 and its slowing down in 1960–1970 are also reflected in the model. These features can be explained by the maximum solar constant and minimum volcanic aerosols in 1940–1950 and by the minimum solar activity and maximum volcanic aerosols in 1960–1970 (Fig. 1). However, it follows from the temperature variation in the control experiment (Fig. 2) that these features can be related to the natural variability of the atmosphere–ocean system. In the literature, it is also shown that these features may be due to both variations in the solar constant and volcanic-aerosol concentrations [24] and the internal variability of the atmosphere–ocean system [25].

Let us compare the temperature variation at the end of the 21st century according to the INM model with the data of other models from [1]. Under scenario B1, the warming in 2091–2110 (with respect to 1991–2010) is 1.7 K in the INM model. According to the data of all models, under this scenario, the warming varies from 1.1 to 2.5 K (the mean value is 1.8 K). For scenario A1B, the warming is 2.3 K according to the INM model data and 1.8–3.8 K (the mean value is 2.8 K) according to the data of all models. For scenario A2, the warming is 3.2 K according to the INM model data and 2.5–4.7 (the mean is 3.6 K) according to the data of all models. For the three scenarios, the warming in the INM model is somewhat less than its mean value over all models, a finding that is in agreement with the data obtained from the experiment on simulation of a nonequilibrium response to doubled CO₂. In the 22nd century, despite the conservation of external forcings at the level of the year 2100, the warming persists and is equal to 0.3 K for scenario B1, 0.5 K for scenario A1B, and 1.5 K for scenario A2. Slight temperature variations during the 22nd century in experiments A1B and especially B1 are due to the fact that the concentration of methane, whose contribution to the greenhouse effect is significant, is decreased in the second half of the 21st century according to these scenarios (Fig. 1). Therefore, despite the increase in CO₂, the climate system by the year 2100 is not very far from equilibrium. At the same time, under scenario A2, increases in the concentrations of CO₂ and methane occur up to the very end of the 21st century; therefore, by the year 2100, the climate system is far from equilibrium, and the warming in the 22nd century under scenario A2 is greater than under scenarios A1B and B1.

Temperature variations under a global warming are nonuniform over the surface. Figure 4 gives the difference of air temperatures at the surface over the years 2151–2200 of experiment A1B and over the years 1951–2000 of experiment 20. The warming is maximum in the Arctic and reaches 10 K. For the territory of Russia, the rise in air temperature is 5–7 K. Over

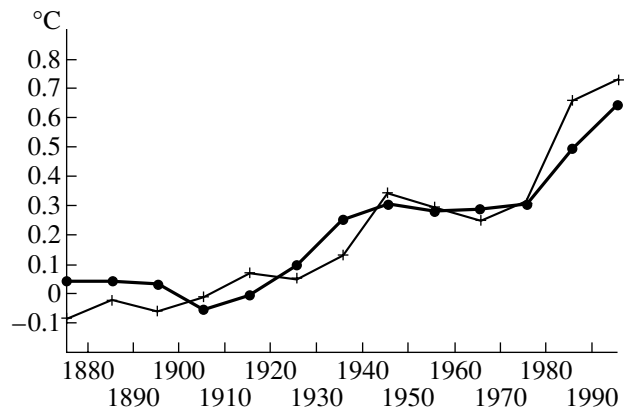


Fig. 3. Variation in globally averaged surface air temperature in 1871–2000 according to observational data [23] (thick curve) and difference between the data obtained in experiment 20 and the control experiment (thin curve). The data are averaged over decades.

the rest of the continent, the rise in temperature is 3–5 K. The lowest rise in air temperature (2–3 K) occurs over the tropical and southern oceans. Such a distribution of warming is characteristic of most of the models and is close to the results obtained by averaging the data of all models participating in the CMIP. In the INM model (Fig. 4), variations in precipitation under warming are also characteristic of most of the models. The precipitation is increased (by 20–40%) in the middle and high latitudes of both hemispheres and also over the tropical Pacific. The precipitation is decreased over most of the subtropics and the tropical Atlantic.

The peaks of warming observed in the Arctic and to the east of the Antarctic Peninsula are due to an intensive sea-ice melting at the end of summer. Figure 5 shows the area of sea ice for the Northern Hemisphere in March and September for the control experiment and experiments 20, B1, A1B, and A2. In March, the ice area remains almost unchanged for the control experiment; only high-frequency oscillations occur, and a small negative trend is noted. In experiments B1, A1B, and A2, the ice area is decreased in March. By the end of the 22nd century, the decrease reaches 20, 30, and 50%, respectively. In September, variations in the area of sea ice are even wider. Even by the end of the 20th century, the ice area in experiment 20 is decreased by 20–25% as compared to the control experiment. In the 22nd century, there is no ice in the Arctic in experiment A2; ice remains until September only in some years in experiment A1B; and, in experiment B1, ice remains, but its area is only 10–20% of that in the control experiment.

According to observational data [26], at the end of the 20th century, in July–September, the area of the Arctic ice was 20–25% less than that in the mid-century and, in January–March, the ice area almost has

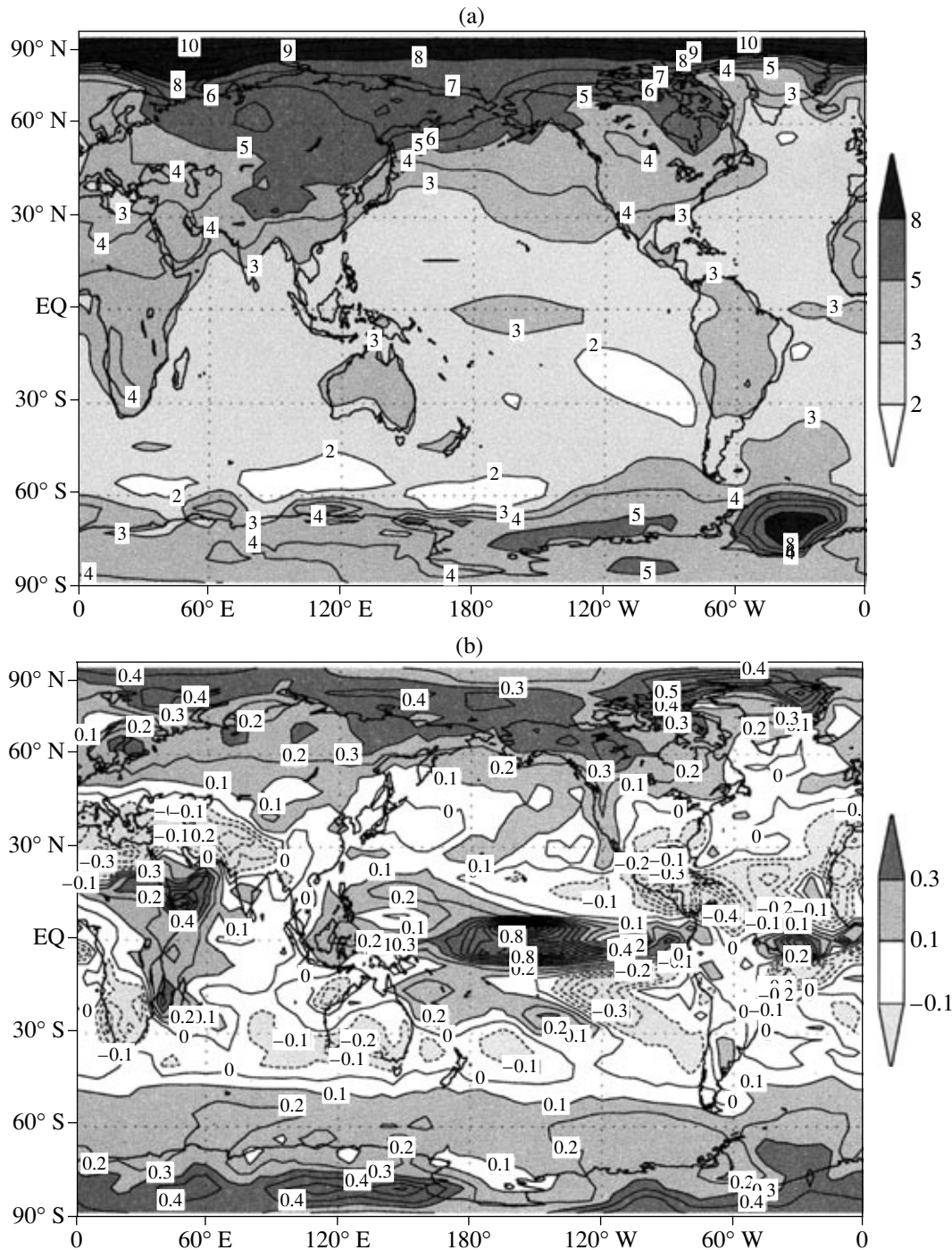


Fig. 4. (a) Temperature variation (K) and (b) relative variation in precipitation (dimensionless) in 2151–2200, experiment A1B, as compared to 1951–2000, experiment 20.

not changed over the past 50 years. This is in agreement with the model data given in Fig. 5.

In Antarctica, the ice area is not decreased as rapidly as in the Arctic (Fig. 6). In September, at the end of the 22nd century, the decrease of ice area is about 20, 30, and 40% for experiments B1, A1B, and A2, respectively. In March, at the end of the 22nd century,

in experiments B1, A1B, and A2, the ice area is 50, 30, and 5%, respectively, of that in the control experiment. In addition, in Antarctica, a significant variability with an amplitude of 20–30% of the mean area is observed for March in the control experiment.

On the basis of the data obtained in experiments 20, 21, B1, A1B, and A2, the response of sea-level

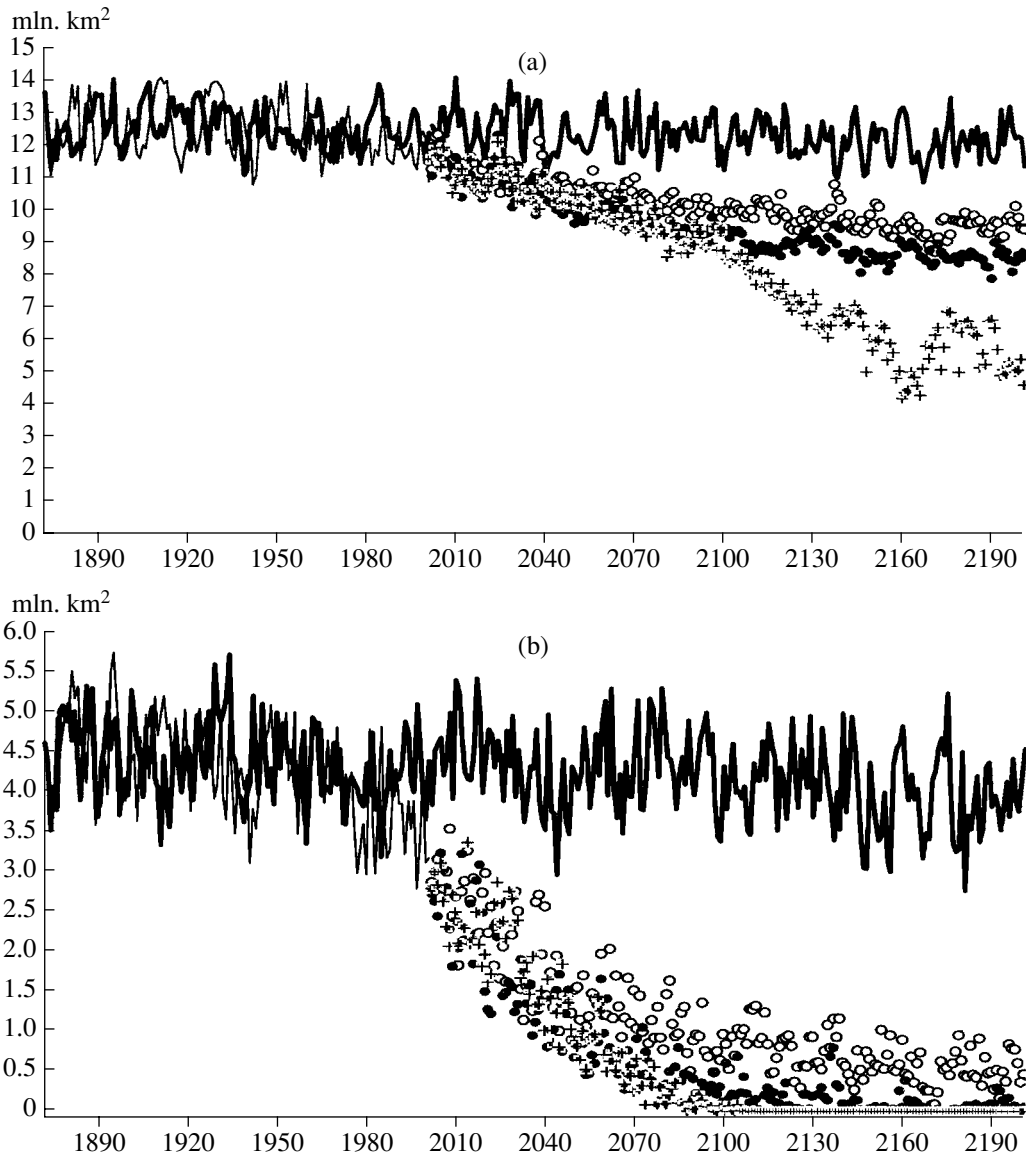


Fig. 5. Sea-ice area in the Northern Hemisphere (mln. km²) for (a) March and (b) September according to the data obtained in the (thick curve) control experiment; (thin line) experiment 20; and (white circles) experiments B1, (black circles) A1B, and (crosses) A2.

variation to variations in external forcings specified in these experiments is calculated. It was assumed that the sea-level variation involves the variations in water density (thermal expansion) and variations in the balance of accumulation and melting of ice in Greenland and Antarctica. To calculate the thermal component, it was assumed that, in 1871, the sea level was equal to 0 m, and the distribution of depth corresponded to that specified in the ocean model. Then, the variation in the mean water density resulting from variations in temperature and salinity and the related variation in sea level were calculated in accordance with the equation of state used in the ocean model.

The contribution made to sea-level variations by the balance of ice in Antarctica and Greenland was calculated in the following way. The amount of precipitation in the form of snow S that had fallen out on the continental ice and the amount of melted ice M were calculated and averaged over 130 years of the control experiment (1871–2000). It was assumed that, in the control experiment, the continental ice is in equilibrium and the amount of ice R broken away from Greenland and Antarctica, on average over 130 years, exactly corresponds to its increase owing to the difference between its accumulation and melting: $R = S - M$. It was assumed that the rate of ice runoff to the ocean R calculated in such a way is the same for any year and

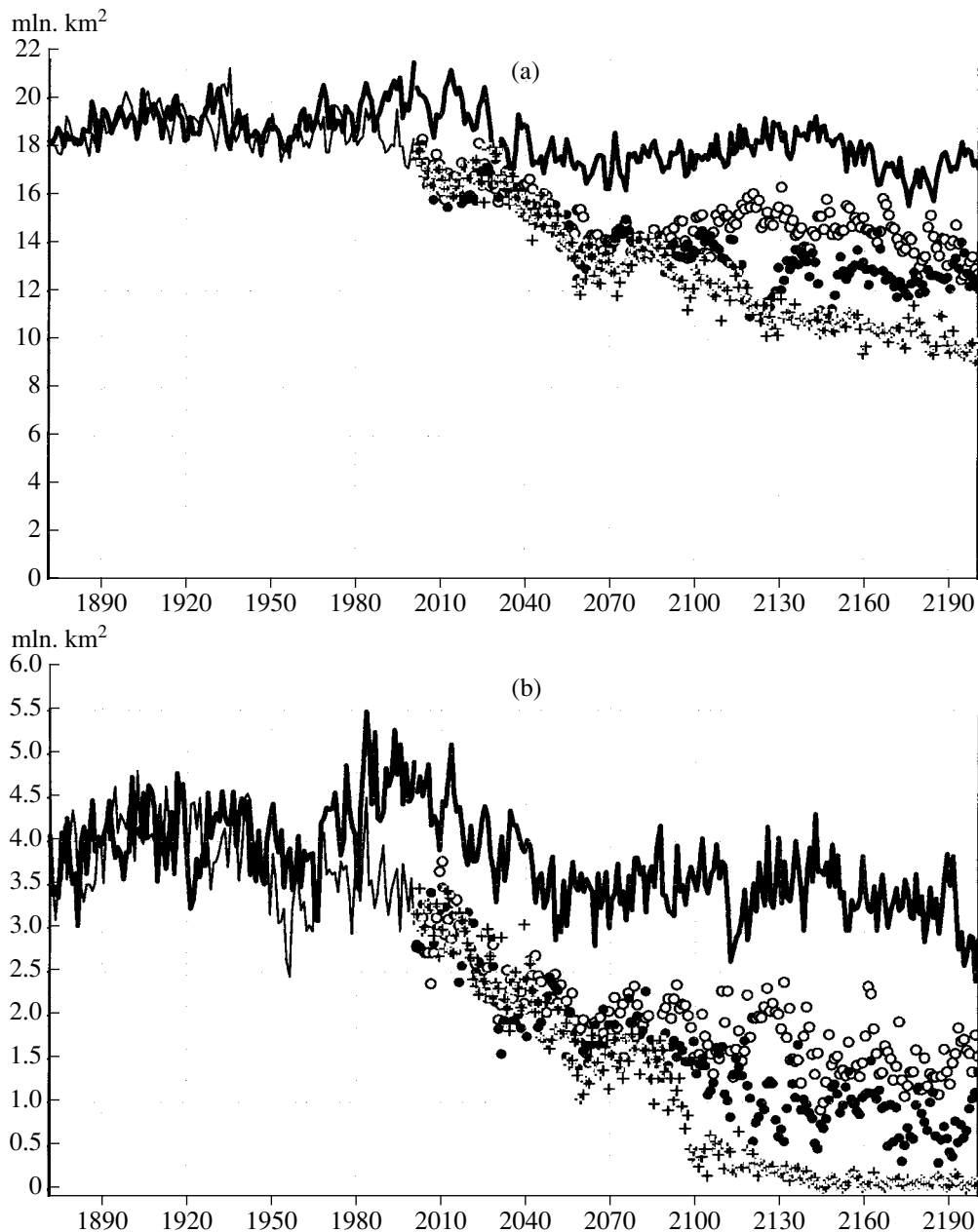


Fig. 6. Sea-ice area in the Southern Hemisphere (mln. km²) for (a) September and (b) March according to the data obtained in the (thick curve) control experiment; (thin line) experiment 20; and (white circles) experiments B1, (black circles) A1B, and (crosses) A2.

for any numerical experiment. The variation in sea level because of variations in the continental-ice balance B was calculated as $B = S - M - R$. The total sea-level variation is the sum of the sea-level variation caused by thermal expansion and the variation of the balance of continental ice.

Figure 7 shows the sea-level variation for experiments 20, 21, B1, A1B, and A2 as compared to the control experiment. According to model data, during the 20th century, the sea-level rise was 4 cm, which is approximately two times less than the estimate

obtained from observational data [1]. The underestimation may be due to the fact that the model does not take into account the melting of small mountain glaciers and that the ocean layer involved in global warming is thinner in the model than in the actual climate system. In experiment 21, the sea level continues to rise and reaches 11 cm by the end of the 21st century. By the end of the 22nd century, the sea-level rise for scenarios B1, A1B, and A2 is 27, 36, and 48 cm, respectively. Owing to a large thermal inertia of the oceans, the sea level continues to rise in the 22nd cen-

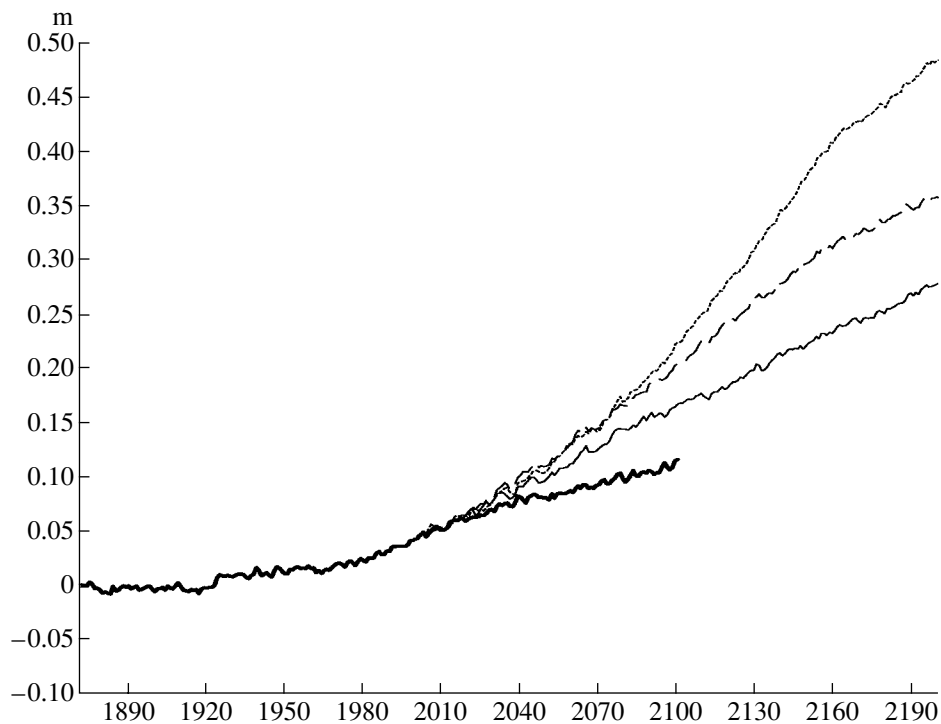


Fig. 7. Variation in sea level (m) for (thick solid curve) experiments 20 and 21, (thin curve) B1, (dashed curve) A1B, and (dotted curve) A2 with respect to the control experiment.

tury, when external forcings are fixed, at a rate almost identical to that in the 21st century. According to model data, the major contribution to the sea-level rise is made by thermal expansion. The contribution of the variation in the balance of ice in Greenland and Antarctica does not exceed 2–3 cm. Moreover, for experiments 21, B1, and A1B, this contribution is mainly negative; i.e., at a comparatively slight global warming, the increase in snowfall exceeds that in the amount of melted snow.

Comparison of the sea-level rise in the INM model with the data obtained with other models and given in [1] shows that, among all models, the INM value is one of the lowest model values. Thus, for all models, the variation in the sea level in 2100 (as compared to 1990) is between 8 and 56 cm for scenario B1, between 13 and 69 cm for scenario A1B, and between 16 and 74 cm for scenario A2. In the INM model, these values are equal to 11, 16, and 18 cm for experiments B1, A1B, and A2, respectively. However, the last model comparison, whose results are to be presented in the fourth IPCC report being prepared, shows that the scatter in model data on this parameter is decreased mainly owing to a decrease in the upper bound of its estimate (J. Gregory 2005, private communication). According to the data obtained with 11 models, the sea-level rise in 2100 as compared to 1990 may vary from 9 to 27 cm for scenario B1, from 12 to 36 cm for scenario A1B, and from 15 to 36 cm for scenario A2. This comparison shows that, in the 20th cen-

tury, the sea-level rise varies from 0 to 7 cm according to the data obtained with all models and is 4 cm according to the INM model. Thus, according to the data of this comparison, the sea-level rise in the INM model is within the same interval. We note that the scatter in the sea-level rise values among the models is wider than that for each individual model but for different scenarios.

2.1. Ocean Response

Here, we will consider the integral characteristics of ocean response. The ocean model as a component of the coupled model has a small trend in deep-sea layers, which is manifested in all characteristics. This trend is due to the features of the ocean model and to some imbalance of the heat and freshwater fluxes on the ocean surface. An incomplete balance between the river runoff and the precipitation is also responsible for this trend. Therefore, to reveal the response of the ocean to global warming, we shall treat its response as the averaged (over the past 30 years) differences in its characteristics obtained from the experiment under the most probable scenario A1B and the control experiment 80. Below, we shall associate these differences with the ocean responses to global warming.

An important factor maintaining the Earth's climatic equilibrium is the meridional heat transfer (MHT) in the ocean. Figure 8a shows the MHT (averaged over the past 30 years of the control experiment 80) for the

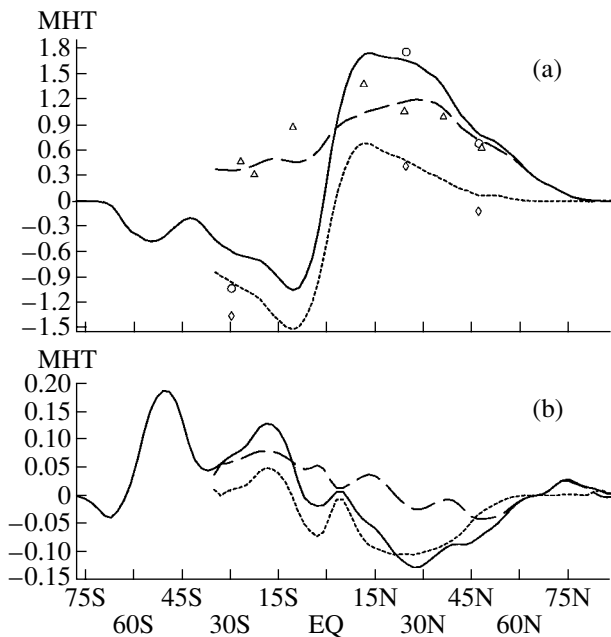


Fig. 8. (a) Meridional heat transfers (MHTs) and (b) their responses in the coupled model for the global ocean (solid curve), the Atlantic (dashed curve), and the Pacific plus Indian oceans (dotted curve). Fig. 8a gives the values of meridional heat transfer from [27] for the global ocean (circles), the Atlantic (triangles), and the Indian and Pacific oceans (rhombuses). The positive MHT values correspond to the northward heat transfer, and the negative values correspond to the southward heat transfer.

global ocean, the Atlantic, and the Pacific plus Indian oceans. Positive and negative MHT values correspond to northward and southward transfers, respectively. The latitude MHT distribution agrees well with the distribution averaged over all CMIP models [1, 4]. For comparison, the MHT values from [27] are given for the global ocean (circles), the Atlantic (triangles), and the Pacific plus Indian oceans (rhombuses), which are in agreement with sparse direct observational data [28]. In the new version of the coupled INM model, the MHT amplitudes were increased, which brought model values closer to observational data. For example, the global MHT was increased approximately by 0.5 PW for both Northern and Southern hemispheres as compared to the previous version of the coupled model [5]. The maximum of the calculated global mean annual MHT is about 1.8 PW for the Northern Hemisphere and -1 PW for the Southern Hemisphere at latitudes of about 10° .

The mean annual heat transfer in the Atlantic (Fig. 8b, dashed curve) reaches its maximum 1.2 PW at 30° N and then decreases with its turning eastward and with a decreased intensity of the Gulf Stream and North Atlantic current. In the Southern Hemisphere, the heat transfer is determined mainly by the processes occurring in the Pacific and Indian oceans. In these oceans, the joint heat transfer to the south (Fig. 8b,

dotted curve) reaches its maximum 1.4 PW at 15° S. It should be noted that the heat transfer is increased in the Northern Hemisphere mainly due to the increased MHT in the Atlantic and in the Southern Hemisphere owing to heat transfer in the Pacific and Indian oceans.

MHT intensification in the ocean is a positive effect of the modernized coupled model. Earlier, its value was among the smallest for the CMIP models. This intensification is caused by an increased intensification of meridional circulation in the upper ocean layers, which, in turn, is increased owing to both the strengthening of trade winds in the coupled model and the change (in numerically implementing the ocean model) to the C grid, which has a lower dissipation than the B grid used in the previous version of the model.

Figure 8b shows the MHT variations caused by climate changes under scenario A1B for the global ocean, the Atlantic, and the Pacific plus Indian oceans. The character of the global response in the MHT is formed so as to decrease the intensity of the global MHT in the control experiment. Figure 8b shows that the response in the global MHT is formed through the responses in the Atlantic and in the Pacific and Indian oceans, which are of quite a different character. In this case, the decrease in the MHT is caused mainly by decreased MHT in the tropics of the Pacific for the Northern Hemisphere and in the tropical Atlantic for the Southern Hemisphere.

The spatial structure of the MHT response can be formed by the responses in the meridional circulation and/or the meridional distribution of ocean temperature. With the exception of a wavelike response in the MHT in the equatorial region, major variations in the MHT are caused by the corresponding variations in meridional circulation in the Atlantic and Pacific oceans (see Fig. 9). This figure shows the responses for the stream function of the zonally averaged circulation in the Atlantic and in the Pacific and Indian oceans against the background of the zonally averaged circulation itself.

It follows from Fig. 9 that the positive response in the MHT in the tropics of the Southern Hemisphere (Fig. 8b) is caused by a positive cell of the response of circulation in the upper layer of the South Atlantic with its center at approximately 15° S and a depth of 400 m, and the negative response in the MHT in the tropics of the Northern Hemisphere is caused by a positive cell of the response of meridional circulation in the upper layer of the Pacific with its center at approximately 15° N and a depth of 300 m. Here, it should be noted that the formation of both the MHT itself and its response is mostly affected by meridional circulation in the upper ocean layer because the near-surface sectors of circulation cells transport the near-surface water, which is warmer than the water transported by their deep-water sectors, and, therefore,

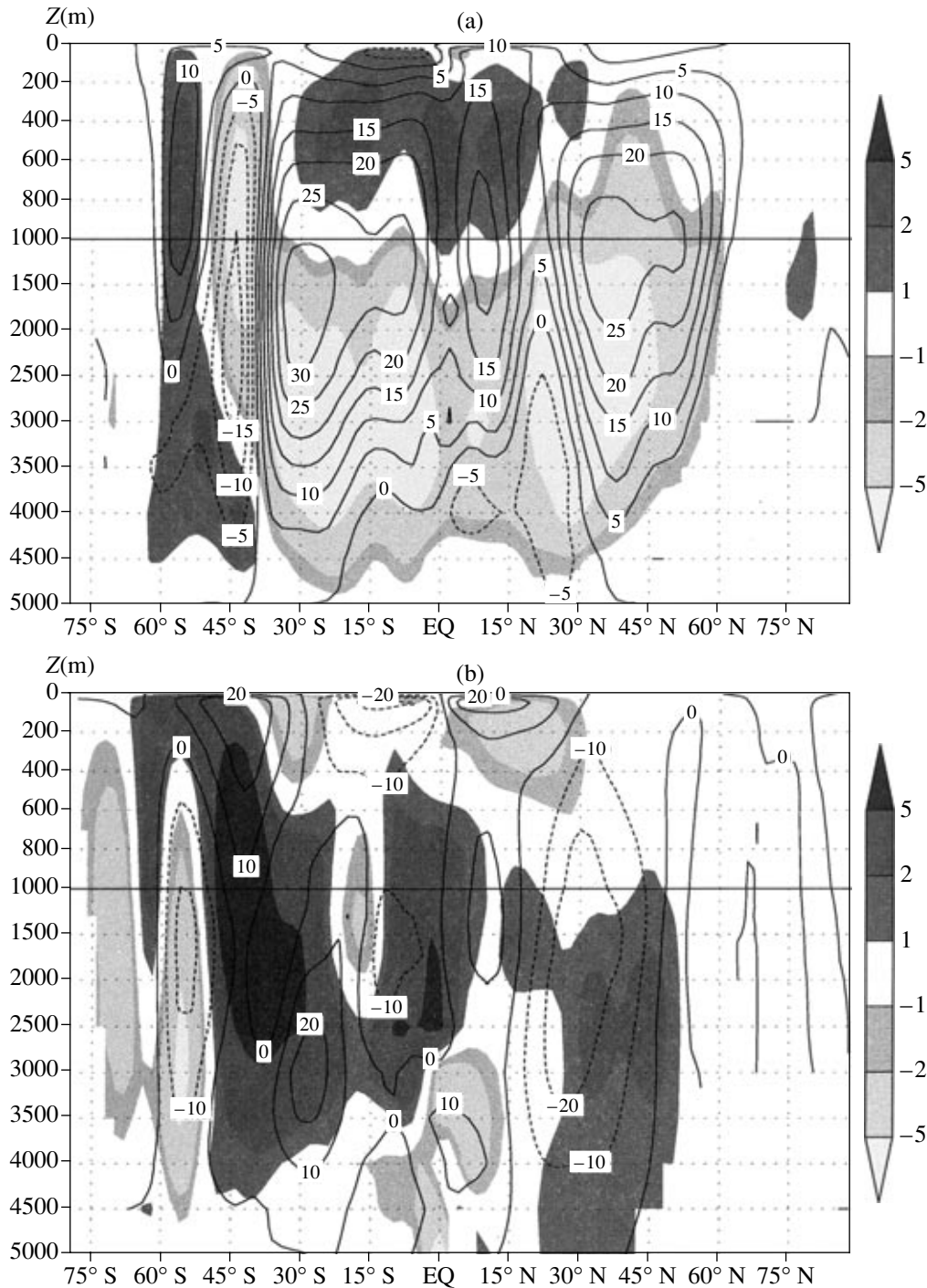


Fig. 9. Stream function of zonally averaged meridional circulation and its response in (a) the Atlantic Ocean and (b) the Pacific plus Indian oceans. The solid contours denote the positive values of the meridional stream function, which correspond to the clockwise motion, and the dashed contours denote the negative values, corresponding to the counterclockwise motion. The response of meridional circulation to increased CO_2 is shown with the aid of shading with the gradation scale on the right.

determine heat transfer to a greater extent. Meridional circulation and its variability in the deep-water ocean layers have a weaker influence on the MHT because this circulation transports the water of deep ocean layers with a weak vertical stratification. Therefore, the

extensive deep-sea negative cell of the response of meridional circulation in the Atlantic Ocean does not significantly affect the MHT. This is also true for meridional circulation in the Pacific and Indian oceans.

A sufficiently significant peak in the response of meridional circulation in the Southern Ocean is caused (as shown in Fig. 9b) mainly by the response in the sector of the Pacific and Indian oceans. This response corresponds to an increase of heat transfer to Antarctica, a phenomenon that must lead to an additional factor of sea-ice melting in this region.

A wavelike response of the MHT in the equatorial region is caused by a significant rise in the OST in this region of the Pacific Ocean (see Fig. 4a), when the warm water of this region is transported by the near-equatorial cells of meridional circulation.

Here, for lack of room, we do not show the response of ocean salinity. Only note that the response of the sea surface salinity is determined primarily by a variation in the surface freshwater balance, a circumstance that is mainly due to variations in precipitation (see Fig. 4b). In this case, the sea surface salinity decreases in the Pacific and mainly increases in the Atlantic (especially in the tropics). Such a redistribution of surface freshwater fluxes must lead to the rise of the sea level in the Pacific and to its decline in the Atlantic. The salinity response is reflected in the meridional freshwater transport, which is formed by both the response of meridional circulation and salinity variations mainly in the upper ocean layers.

CONCLUSIONS

The INM coupled atmosphere–ocean general circulation model was used to conduct experiments on the simulation of climate changes under doubled and quadruple CO_2 concentrations; the climate of the 20th century under prescribed variations in external forcings; and climate changes in the 21st–22nd centuries under scenarios B1, A1B, and A2, and the control experiment 330 years in duration for the conditions of the year 1871. In the INM model, the nonequilibrium sensitivity to doubled CO_2 is somewhat lower than its mean value over all models and is equal to 1.57 K. However, the equilibrium sensitivity of the atmosphere model with a homogeneous 50-m ocean layer is the lowest among the models under consideration and is equal to 2.1 K. The model adequately reproduces observed variations in surface air temperature for 1871–2000. In the model, the warming over the 20th century is 0.7 K, which is close to observational data.

The features of the observed time variation in air temperature such as warming in 1940–1950 and its slowing down in 1960–1970 are reproduced by the model. According to model data, the increase in the mean air temperature at the surface at the end of the 22nd century as compared to the end of the 20th century is about 2, 3, and 5 K for scenarios B1, A1B, and A2, respectively. This is slightly lower than the mean value for all models used in such experiments [1]. The

maximum warming occurs in the Arctic. For all scenarios, in the model, the sea-ice area in the Arctic is significantly reduced at the end of summer and, for scenarios A1B and A2, in the 22nd century, the Arctic ice almost completely melts by the end of summer. In the model, the sea-level rise in 2100 as compared to 1990 is 11 cm, 16 cm, and 18 cm for scenarios B1, A1B, and A2, respectively. These are among the lowest values for the models whose results are given in [1].

The response of the MHT to global warming is formed mainly owing to the changes occurring in the pattern of meridional circulation and heat store in the tropics of the Pacific. The response in the Atlantic suggests a strengthening of the northward heat flux. Conversely, the southward heat transfer is strengthened in the Pacific and Indian oceans. A significant peak is observed in the response of the meridional circulation in the Southern Ocean. This peak corresponds to an increased heat transfer to Antarctica and is caused mainly by the response in the sector of the Pacific and Indian oceans.

In conclusion, we note that the correct reproduction of the time variation in air temperature for the 20th century does not guarantee that the model predictions for the 21st–22nd centuries, even under the assumption that one of the aforementioned scenarios of variations in external forcings is exactly fulfilled, will also be correct. This result is due to the fact that there are great uncertainties in estimating variations in radiation forcing for the 20th century, which are associated primarily with an uncertainty in a sulfate-aerosol forcing, whose estimates vary from 0 to 2 W/m^2 [1]. Therefore, an incorrect sensitivity of the model to variations in the concentrations of greenhouse gases can be compensated by incorrect variations in the radiation forcing from sulfate aerosol and, as a result, the reproduction of warming in the 20th century may prove to be correct. According to the scenarios under consideration, in the 21st century, the concentration of greenhouse gases will be increased, while the concentration of sulfate aerosol will be increased only at the beginning of the 21st century and then will be decreased (Fig. 1). Therefore, it is not improbable that the model correctly reproducing the warming in the 20th century can underestimate or overestimate the warming in the 21st–22nd centuries.

ACKNOWLEDGMENTS

We are grateful to V.P. Dymnikov for helpful advice and his interest in the development and operation of the INM RAS coupled model.

This study was supported by the Russian Foundation for Basic Research (project nos. 06-05-64331-a, 06-05-64246-a) and the fundamental research program No. 17 “Parallel Calculations and Multiproces-

sor Calculation Systems” of the Presidium of the Russian Academy of Sciences.

REFERENCES

1. *Climate Change 2001. The Scientific Basis. Intergovernmental Panel on Climate Change*, Ed. by J. T. Houghton, Y. Ding, D. J. Griggs, et al. (Cambridge, 2001).
2. V. P. Dymnikov and A. N. Filatov, *Principles of Mathematical Theory of Climate* (VINITI, Moscow, 1994) [in Russian].
3. M. I. Budyko, *Climate in the Past and Future* (Gidrometeoizdat, Leningrad, 1980) [in Russian].
4. C. Covey, K. M. AchutaRao, S. J. Lambert, and K. E. Taylor, “Intercomparison of Present and Future Climates Simulated by Coupled Ocean–Atmosphere GCMs,” PCMDI Report, No. 66, 1–20 (2000).
5. N. A. Diansky and E. M. Volodin, “Simulation of Present-Day Climate with a Coupled Atmosphere–Ocean General Circulation Model,” *Izv. Akad. Nauk, Fiz. Atmos. Okeana* **38**, 824–840 (2002) [*Izv., Atmos. Ocean. Phys.* **38**, 732–747 (2002)].
6. E. M. Volodin and N. A. Diansky, “Simulation of El Niño in a Coupled Ocean–Atmosphere General Circulation Model,” *Meteorol. Gidrol.*, No. 12, 5–14 (2004).
7. V. P. Dymnikov, V. N. Lykosov, E. M. Volodin, et al., “Current Problems of Numerical Mathematics and Mathematical Modeling. Modeling Climate and Its Changes,” in *Collection of Papers in Two Volumes Devoted to the 80th Birthday of G.I. Marchuk and 25th Anniversary of the INM RAS* (Nauka, Moscow, 2005), Vol. 2, pp. 13–137 [in Russian].
8. E. M. Volodin and N. A. Diansky, “Response of a Coupled Atmosphere–Ocean General Circulation Model to Increased Carbon Dioxide,” *Izv. Akad. Nauk, Fiz. Atmos. Okeana* **39**, 193–210 (2003) [*Izv., Atmos. Ocean. Phys.* **39**, 170–186 (2003)].
9. V. A. Alekseev, E. M. Volodin, V. Ya. Galin, et al., “Modeling Present-Day Climate with the INM RAS Atmospheric Model,” Preprint No. 2086-V98, INM (1998).
10. V. Ya. Galin, E. M. Volodin, and S. P. Smyshlyaev, “INM RAS Atmospheric General Circulation Model with Ozone Dynamics,” *Meteorol. Gidrol.*, No. 5, 13–23 (2003).
11. V. Ya. Galin, “Parametrization of Radiative Processes in the DNM Atmospheric Model,” *Izv. Akad. Nauk, Fiz. Atmos. Okeana* **34**, 380–389 (1998) [*Izv., Atmos. Ocean. Phys.* **34**, 339–347 (1998)].
12. A. K. Betts, “A New Convective Adjustment Scheme. Part I. Observational and Theoretical Basis,” *Q. J. R. Meteorol. Soc.* **112**, 677–691 (1986).
13. E. M. Volodin and V. N. Lykosov, “Parametrization of Heat and Moisture Transfer in the Soil–Vegetation System for Use in Atmospheric General Circulation Models: 1. Formulation and Simulations Based on Local Observational Data,” *Izv. Akad. Nauk, Fiz. Atmos. Okeana* **34**, 453–465 (1998) [*Izv., Atmos. Ocean. Phys.* **34**, 405–416 (1998)].
14. T. N. Palmer, G. J. Shutts, and R. Swinbank, “Alleviation of a Systematic Westerly Bias in General Circulation and Numerical Weather Prediction Models through an Orographic Gravity Wave Drag Parameterization,” *Q. J. R. Meteorol. Soc.* **112**, 1001–1031 (1986).
15. C. O. Hines, “Doppler Spread Parameterization of Gravity Wave Momentum Deposition in the Middle Atmosphere. Part 2. Broad and Quasimonochromatic Spectra, and Implementation,” *J. Atmos. Solar Terr. Phys.* **59**, 387–400 (1997).
16. N. A. Diansky, A. V. Bagno, and V. B. Zalesny, “Sigma Model of Ocean Global Ocean Circulation and Its Sensitivity to Variations in Wind Stress,” *Izv. Akad. Nauk, Fiz. Atm. Okeana* **38**, 537–556 (2002) [*Izv., Atmos. Ocean. Phys.* **38**, 477–494 (2002)].
17. A. S. Sarkisyan, V. B. Zalesny, and N. A. Diansky, “Current Problems of Numerical Mathematics and Mathematical Modeling. Mathematical Models of Ocean and Sea Circulation,” in *Collection of Papers in Two Volumes Devoted to the 80th Birthday of G.I. Marchuk and 25th Anniversary of the INM RAS* (Nauka, Moscow, 2005), Vol. 2, pp. 174–276 [in Russian].
18. G. I. Marchuk, *Methods of Numerical Mathematics*, 2nd ed. (Nauka, Moscow, 1980; Springer, New York, 1975).
19. R. C. Pacanovsky and G. Philander, “Parametrization of Vertical Mixing in Numerical Models of the Tropical Ocean,” *J. Phys. Oceanogr.* **11**, 1442–1451 (1981).
20. N. G. Yakovlev, “Coupled Model of Ocean General Circulation and Sea Ice Evolution in the Arctic Ocean,” *Izv. Akad. Nauk, Fiz. Atm. Okeana* **39**, 394–409 (2003) [*Izv., Atmos. Ocean. Phys.* **39**, 355–368 (2003)].
21. M. Steele, R. Morley, and W. Ermold, “A Global Ocean Hydrography with a High Quality Arctic Ocean,” *J. Clim.* **14**, 2079–2087 (2001).
22. E. M. Volodin and CMIP member groups, “Relation between the Global-Warming Parameter and the Heat Balance on the Earth’s Surface at Increased Contents of Carbon Dioxide,” *Izv. Akad. Nauk, Fiz. Atmos. Okeana* **40**, 306–313 (2004) [*Izv., Atmos. Ocean. Phys.* **40**, 269–275 (2004)].
23. P. D. Jones, M. New, D. E. Parker, et al., “Surface Air Temperature and Its Changes over the Past 150 Years,” *Rev. Geophys.* **37**, 173–199 (1999).
24. G. A. Meehl, W. M. Washington, C. M. Ammann, et al., “Combination of Natural and Anthropogenic Forcings in Twentieth-Century Climate,” *J. Clim.* **17**, 3721–3727 (2004).
25. A. J. Broccoli, K. W. Dixon, T. L. Delworth, et al., “Twentieth-Century Temperature and Precipitation Trends in Ensemble Climate Simulations Including Natural and Anthropogenic Forcing,” *J. Geophys. Res.* **108**, 4798–4812 (2003).
26. A. M. Waple, R. C. Schnell, and R. S. Stone, “State of Climate in 2003. Polar Climate,” *Bull. Am. Meteorol. Soc.* **85**, 29–S34 (2004).
27. A. M. Macdonald and C. Wunsch, “An Estimate of Global Ocean Circulation and Heat Fluxes,” *Nature* **382**, 436–439 (1996).
28. M. M. Hall and H. L. Bryden, “Direct Estimates and Mechanisms of Ocean Heat Transport,” *Deep-Sea Res.* **29**, 339–359 (1982).

Translated by B. Dribinskaya